Math. Model. Nat. Phenom.
Vol. 5, No. 1, 2010, pp. 106-122
DOI: 10.1051/mmnp/20105105

The Role of Cell-Cell Adhesion in the Formation of Multicellular Sprouts

A. Szabó[1] **and A. Czirók** [2,1] *

[1] Department of Biological Physics, Eötvos University, Budapest, Hungary
[2] Department of Anatomy & Cell Biology, University of Kansas Medical Center Kansas City, KS, USA

Abstract. Collective cell motility and its guidance via cell-cell contacts is instrumental in several morphogenetic and pathological processes such as vasculogenesis or tumor growth. Multicellular sprout elongation, one of the simplest cases of collective motility, depends on a continuous supply of cells streaming along the sprout towards its tip. The phenomenon is often explained as leader cells pulling the rest of the sprout forward via cell-cell adhesion. Building on an empirically demonstrated analogy between surface tension and cell-cell adhesion, we demonstrate that such a mechanism is unable to recruit cells to the sprout. Moreover, the expansion of such hypothetical sprouts is limited by a form of the Plateau-Taylor instability. In contrast, actively moving cells – guided by cell-cell contacts – can readily populate and expand linear sprouts. We argue that preferential attraction to the surfaces of elongated cells can provide a generic mechanism, shared by several cell types, for multicellular sprout formation.

Key words: sprouting, leader cell, Potts model
AMS subject classification: 92C15, 92C17, 92C37

1. Introduction

The collective motility of interconnected cells is a poorly understood, but fundamental, process during development [32]. Arguably, cell sorting is the best studied process involving simultaneous displacement of closely packed cells [38, 49]. The differential adhesion hypothesis and its computational representations – based on the Potts model [18, 24] or analogous lattice-free variants [35, 4] – successfully explain the outcome as well as the time-course of cell sorting experiments

*Corresponding author. E-mail: aczirok@kumc.edu

[1]. However, the cell types used in sorting experiments move diffusively within bulk, uniform environments far from cell type boundaries [38], although some temporal and spatial correlations are detectable [49].

Less is known how polarized cells, i.e., cells that maintain their directional motility in time, coordinate their motility during collective migration. As reviewed in [14] and [32], the collective movement of cell chains, sprouting, is of great importance during development and in certain diseases such as tumor growth. Multicellular sprouting is often considered as a special case of sheet migration, the expansion process of a monolayer into an empty area or "wound". During sheet migration cells at the boundary exert substantial traction forces [10] and are thought to pull the passive bulk of the sheet forward [9]. Similarly, cells participating in sprout formation are often divided into two subpopulations and the process is explained as *leader cells* pulling a gliding bulk of passive, *"stalk"* cells by means of cell-cell adhesion [14]. The assumption that the stalk population is not participating in active cell motion is based on observations that these cells have few connections with the extracellular matrix (ECM) environment [14], or lack filopodia [17].

We argue, that the above view is inconsistent with the widely accepted models of cell-cell adhesion. In particular, cadherin-mediated cell-cell adhesion has been repeatedly shown to be analogous to surface tension [12, 11, 5, 13, 21], and has been modeled accordingly in theoretical studies [18, 24, 35]. Surface tension-stabilized structures are, however, prone to the Plateau-Rayleigh instability: a liquid jet with a circular cross-section should break up into drops if its length exceeds its circumference [8, 23]. Due to this instability, as we demonstrate below, a sprout pulled by a leader cell should also break up. Therefore, multicellular sprouting cannot be fully accounted for solely by the presence of leader cells and cell-cell adhesion. Instead, we suggest that while stalk cells may be detached from the matrix, due to cell-guided motility their motion should not be entirely passive – and in the presence of autonomous cell motility the arguments for the Plateau-Rayleigh instability do not apply.

Motility analysis of certain cell cultures revealed that stalk (sprout) cell surfaces are more attractive migration targets than the surfaces of well-spread cells in the aggregate bulk [45]. As cells in the sprout tend to be elongated, we proposed that cells attach preferentially to elongated cells [46]. While the underlying molecular mechanism is unclear, micromechanical differences between sprout and well-spread cells [26] and their detection through mechano-sensing may represent a plausible potential mechanism. Utilizing computer simulations, preferential attraction to elongated cells has been shown to result in network assembly within a system of initially scattered cells. However, as we demonstrate below and in Fig. 8 of [6], our formerly proposed models could not adequately reproduce multicellular sprouting from a reservoir of adherent cells as (i) movement of the sprout tip is not sufficiently persistent resulting in curved branches; (ii) the previously formed sprout bodies move sideways; and (iii) the speed of expansion diminishes over time. In this study we explore a cell-autonomous mechanism (i.e., a mechanism independent of extracellular chemical or mechanical guidance fields) for multicellular sprouting that utilizes both the leader-cell concept and the preferential attachment of cells to elongated neighbors.

2. Empirical data

In experimental systems, where sprouting activity has been analyzed in detail, active and passive cell states can be, indeed, distinguished based on the degree of cellular motility. During the formation of the early vasculature in quail embryos clusters of non-motile cells are maintained while highly motile multicellular sprouts invade avascular areas [39, 6]. In mouse allantois explants rapidly migrating sprout precursor cells appear within a cluster of cells lacking autonomous motility [36]. In cultures of C6 cells linear branches contain highly motile cells whereas cells remain non-motile in the well-spread, isotropic clusters [45].

By analyzing published image sequences, in Fig. 1 we demonstrate that the speed of sprout expansion is steady in each of these cases. Furthermore, the sprout is often surprisingly "fluid", i.e., cells move with different velocities and thus the order of cells within the sprout can be changed.

3. Cellular Potts Model of interacting, motile cells

We analyze cell-guided sprouting by means of a two dimensional Cellular Potts Model (CPM), a frequently used method to deal with movements of close packed cells [18, 24]. The main advantage of the CPM approach is that cell shape is explicitly represented, thus the simulation can resolve cell intercalation, an important mode of configuration rearrangement. To obtain a biologically plausible, yet simple model, we augment the CPM with cell-autonomous motility.

The CPM is defined on a lattice, where each lattice site is labeled with an integer σ. Cells are represented as simply connected domains, i.e., a set of adjacent lattice sites sharing the same label σ, equal to the cell index i ($0 < i \leq N$, where N is the number of cells in the simulation). Furthermore, we also distinguish arbitrarily shaped cell free areas, where $\sigma = 0$.

Cell movement is resulted from a series of elementary steps. Each step is an attempt to copy the label value from a random lattice site $\mathbf{a}$ to an adjacent site $\mathbf{b}$. This elementary step is executed with a probability $p(\mathbf{a} \to \mathbf{b})$. If the domains remain simply connected, thus cells do not break apart or form holes, the probability assignment rule ensures (i) the maintenance of a target cell size, (ii) adhesion of cells and (iii) active cellular motion:

$$\ln p(\mathbf{a} \to \mathbf{b}) = \min[0, -\Delta H(\mathbf{a} \to \mathbf{b}) + w(\mathbf{a} \to \mathbf{b})], \tag{3.1}$$

where w is a bias responsible for the specific dynamics considered and H is a goal function to be minimized. The difference $\Delta H(\mathbf{a} \to \mathbf{b})$ is obtained by evaluating H both at the current configuration and at the configuration obtained after the elementary step $\mathbf{a} \to \mathbf{b}$ has been applied.

Since updating each lattice position takes more steps in a larger system, the elementary step cannot be chosen as a unit of real time. Instead, the usual choice for time unit – the Monte Carlo step (MCS) – is L^2 elementary steps, where L is the linear system size [30, 3].

Cell-cell adhesion, cell compressibility and cell boundary roughness are controlled through the CPM Hamiltonian [18] as

$$H = \sum_{\mathbf{x},\mathbf{x}':|\mathbf{x}-\mathbf{x}'|=1} J_{\sigma(\mathbf{x}),\sigma(\mathbf{x}')} + \lambda \sum_{k=1}^{N} \delta A_k^2. \tag{3.2}$$

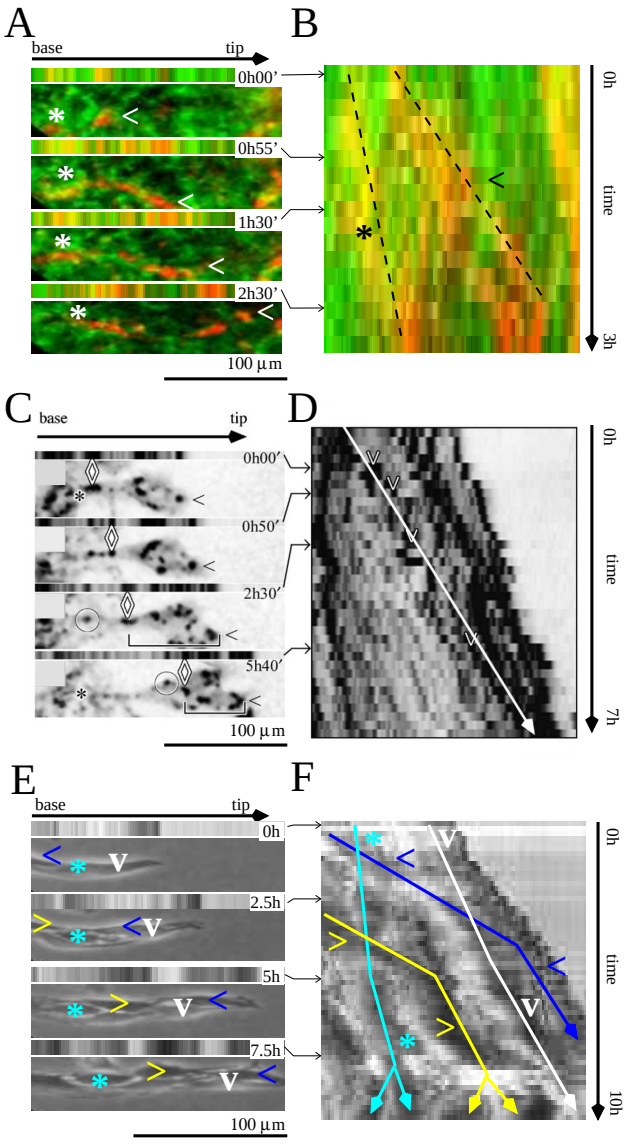

Figure 1: Multicellular sprout expansion in three experimental systems. Panels A, C and E show cell configurations at various time points. Panels B, D and F show intensity profiles along the linear structure for each frame recorded, therefore, in these plots moving objects appear as tilted lines. Tip cells are marked with a caret (<), while an asterisk (*) denotes a cell at the approximate position of the sprout base. The expansion of the sprout is linear in time in all three systems. A,B: QH1-labeled endothelial cells (red) form a vascular segment during vasculogenesis in a HH stage 7 quail embryo (data re-analyzed from [6]). Surrounding tissue movements are visualized by changes in the ECM component Fibrillin-2 (green). The area shown in panel A co-moves with the surrounding ECM. C,D: CD34-labeled cells of a mouse allantoic explant (after [36]). A cell moving from the middle of the sprout to the tip is marked with a diamond. E,F: expansion of a two-cell-wide linear sprout in cultures of C6 cells (data re-analyzed from [45]). The initial tip cell (marked 'v') is taken over by a faster migrating cell (marked '<'). The latter cell slows down after reaching the tip, and thus the overall sprout elongation speed remains unchanged.

The first term in Eq. (3.2) enumerates cell boundary lengths. The summation goes over adjacent lattice sites, and the $J_{i,j}$ interaction matrix $(0 \leq i, j \leq N)$ is given as

$$J_{i,j} = \begin{cases} 0, & \text{for } i = j \\ \alpha, & \text{for } ij > 0 \text{ and } i \neq j \text{ (cell-cell boundary)} \\ \beta, & \text{for } ij = 0 \text{ and } i \neq j \text{ (free cell boundary).} \end{cases} \tag{3.3}$$

The surface energy-like parameters α and β characterize cell-cell adhesions and cell surface fluctuations in the model. The magnitude of these values determines the roughness of cell boundaries: small magnitudes allow dynamic, long and hence curvy boundaries, while large magnitudes restrict boundaries to straight lines and thus freeze the dynamics. This correlation between measured surface energies and cell surface roughness has been elegantly demonstrated with tumor spheroids [21]. The parameter $2\beta - \alpha$ specifies the preference of cell-cell connections over cell-medium boundaries: free cell boundaries are penalized for $2\beta > \alpha$ [19].

The second term in Eq. (3.2) is responsible to maintain a preferred cell area: for each cell k the deviation of its area from a pre-set value is denoted by δA_k. Cellular compressibility is set by λ^{-1}.

We refrain from using a temperature-like parameter, as rule (3) of [18], analogous to our rule (3.1), simply scales each CPM parameter α, β and λ by the temperature, a constant. Thus, when comparing our studies with those that include a temperature in the simulations, our parameter values are to be compared with the corresponding values divided by the temperature.

While H evaluates configurations, w is assigned directly to the elementary step and thus allows the specification of a broad spectrum of cellular behavior. Here we consider three effects and thus compose w as $w_1 + w_2 + w_3$, where the terms describe (1) cell polarization and the resulting persistent directional motility [44], (2) non-uniform membrane dynamics along the cell perimeter, and (3) the preferred attachment to elongated cells [45], respectively.

Cellular self-propulsion is introduced through the cell polarity vector $\mathbf{p}_k$, which represents spatial differences in the biochemical state of cell k [27] and alters the probability assigned to elementary steps according to [44]:

$$w_1(\mathbf{a} \to \mathbf{b}) = \sum_{k=1}^{N} P_k \frac{\mathbf{p}_k}{|\mathbf{p}_k|}(\mathbf{b} - \mathbf{a}), \tag{3.4}$$

where P_k sets the magnitude of autonomous motility (Fig. 2). Motivated by statistical analyses of single cell motility data [41], we propose to update the cell polarity vectors by considering a spontaneous decay and a reinforcement from cell displacements. In each MCS the change in $\mathbf{p}_k$ is

$$\Delta\mathbf{p}_k = -r_k\mathbf{p}_k + \Delta\mathbf{x}_k, \tag{3.5}$$

where r_k is the rate of spontaneous decay and $\Delta\mathbf{x}_k$ is the displacement of the center of cell k during the MCS considered. A characteristic memory length T_k of the polarization vector is defined as $T_k = 1/r_k$. Therefore, we propose a positive feedback loop involving cell movement and polarity [44]. This loop may correspond to the established molecular feedback regulation of the activation

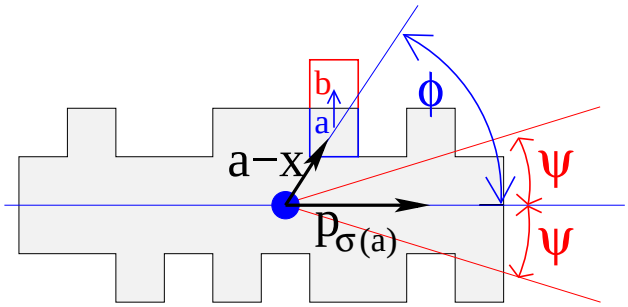

Figure 2: Cell polarity vector and an elementary step. In the elementary step depicted (blue arrow) the site index $\sigma(\mathbf{a})$ at lattice site $\mathbf{a}$ is copied to site $\mathbf{b}$, resulting in the expansion of cell $i = \sigma(a)$. The probability of the $\mathbf{a} \to \mathbf{b}$ step depends on both its location and direction. According to Eq. (3.4), the direction $\mathbf{b} - \mathbf{a}$ is projected onto the normalized polarity vector of the cell, $\mathbf{p}_{\sigma(a)}$. Eq. (3.6) increases membrane fluctuations at the front of the cell, while attenuates elsewhere. The width of the leading edge is 2ψ radians, measured from the cell's center of mass ($\mathbf{x}$, blue dot) and polarity vector direction $\mathbf{p}_{\sigma(\mathbf{a})}$. As the elementary step considered is at site $\mathbf{a}$, the angle between $\mathbf{a} - \mathbf{x}$ and $\mathbf{p}_{\sigma(\mathbf{a})}$ is ϕ.

of rho GTPases and processes involved in cellular motility such as expansion of the cytosol and polymerization of cytoskeletal elements [50, 37, 7].

Cell polarity also controls cell shape changes as membrane dynamics is more pronounced at the leading edge and inhibited at the sides and trailing edge [27]. Thus, if ψ is the half-width of the leading edge, $\mathbf{p}_{\sigma(\mathbf{a})}$ is the polarity vector of cell $\sigma(a)$ (which contains lattice site a, see Fig. 2), we assume

$$w_2(\mathbf{a} \to \mathbf{b}) = S_{\sigma(\mathbf{a})} f(\psi - \phi(\mathbf{p}_{\sigma(\mathbf{a})}, \mathbf{a} - \mathbf{x}_{\sigma(\mathbf{a})})). \tag{3.6}$$

In Eq. (3.6) S_k sets the magnitude of this effect for cell k, $\phi(\mathbf{u}, \mathbf{v})$ denotes the absolute value of the angle between the vectors $\mathbf{u}$ and $\mathbf{v}$, and $f(\alpha) = 2\Theta(\alpha) - 1$ is conveniently constructed using a Heaviside function $\Theta(\alpha)$. Notice, that w_2 depends only on $k = \sigma(\mathbf{a})$, the expanding cell.

Finally, w_3 describes the preferential attachment to elongated cells as introduced in [45]:

$$w_3(\mathbf{a} \to \mathbf{b}) = [\chi_{\sigma(\mathbf{a})} - \chi_{\sigma(\mathbf{b})}] \sum_{\substack{\mathbf{c}:|\mathbf{b}-\mathbf{c}|=1 \\ \sigma(\mathbf{c}) \notin \{\mathbf{0}, \sigma(\mathbf{a}), \sigma(\mathbf{b})\}}} \theta_{\sigma(\mathbf{c})}, \tag{3.7}$$

where for cell k the strength of preference is set by χ_k, and θ_k is its measure of anisotropy. As $\chi_0 = 0$, the $\chi_{\sigma(\mathbf{a})} - \chi_{\sigma(\mathbf{b})}$ expression ensures that only cells (and not the medium) exhibit the preference. For $\sigma(\mathbf{a}) = 0$ and $\sigma(\mathbf{b}) > 0$ the elementary step considered is a cell retraction, while for $\sigma(\mathbf{a}) > 0$ and $\sigma(\mathbf{b}) = 0$ the step represents cell expansion. These steps may involve loosing or gaining contact with a distinct cell at an adjacent lattice site $\mathbf{c}$: the summation in Eq. (3.7) goes over those neighboring sites of $\mathbf{b}$ that belong to cells other than $\sigma(\mathbf{a})$ and $\sigma(\mathbf{b})$. For instance, if cell $\sigma(\mathbf{a})$ attempts to move next to cell $\sigma(\mathbf{c})$, and the separating site is empty ($\sigma(\mathbf{b}) = 0$) and no other cell is near to site $\mathbf{b}$, then $w_3 = \chi_{\sigma(\mathbf{a})}\theta_{\sigma(\mathbf{c})}$. Therefore, the probability $p(\mathbf{a} \to \mathbf{b})$ is increased

if $\theta_{\sigma(\mathbf{c})}$ is high. The measure of anisotropy is obtained from the inertia tensor of the lattice domain representing the cell k as $\theta_k = \sqrt{\mu_k/\nu_k} - 1$, where $\mu_k \geq \nu_k$ are the two eigenvalues of the inertia tensor.

4. Simulations

Multicellular sprout expansion was studied with numerical simulations using a suitably modified version of the CPM code of [30]. Simulations were initiated from compact aggregates of 25-50 cells. The linear system size, $L = 300$, was chosen as sufficiently large to allow sprout extension without interaction with the boundaries.

Spatial and temporal calibration of the model has been performed in [44] by comparing simulated monolayers with time-lapse recordings of endothelial cultures plated at high cell density. Cell areas were set to 50 lattice sites, which calibrates the lattice distance to $\approx 5\mu$m. Computational time was measured in Monte Carlo steps (MCS), i.e., L^2 spin conversion attempts [30]. Based on the comparison of the average cell speeds of simulated and experimentally observed [43, 44] cells, 1 MCS corresponds to $\approx$ 1 minute in real time – a value similar to the ones used in other CPM studies [30, 3].

Equations (3.2)-(3.7) contain 8 parameters which describe the behavior of model cells: α (cost associated with cell-cell contacts), β (cost associated with free cell surfaces), λ^{-1} (2D compressibility), P (self-propulsion activity), T (polarity vector memory length), S (coupling between boundary activity and cell polarity), ψ (half-width of the leading edge) and χ (preference for elongated cells). The first three of these defines the basic CPM [18], P and T is our representation of active cell motility analyzed in detail in [44], and the last three parameters correspond to the specific cell behavior patterns we model.

As we model a homogeneous cell population, we assign the same set of parameter values to each cell. The only exception is the persistence time, which is used to distinguish leader and passive cells. Thus, we assume that the polarization of passive cells decays almost instantaneously ($T_{passive} = 1$ MCS), while the polarization is quite persistent in leader cells ($T_{leader} = 500$ MCS). Polarization, therefore, has no substantial effect on the motion of passive cells: they lack directed motion and perform a random walk in the absence of cell-cell interactions (data not shown).

The compressibility λ^{-1} does not play a role in the sprouting processes considered here, thus we fixed $\lambda = 1$. The surface energy-like quantities α and β are, however, in the focus of this study. Their magnitudes set the flexibility of cell interfaces. As the chance for a spontaneous fluctuation (the creation of a one-lattice-site bulge) at the free cell boundary is $\exp(-2\beta)$, in accord with the literature [38, 2, 3] we considered values in the range $0 < \beta \leq 6$ and $\alpha \in \{1, 2\}$.

5. Results

5.1. Cell-cell adhesion alone is insufficient to maintain cell supply to expanding sprouts

By setting $w_3 \equiv 0$, we studied the ability of leader cells to recruit cells into the sprout by relying on the well understood, surface tension-like cell-cell adhesion alone. Simulations were performed with leader and passive cells for a wide range of the CPM parameters α and β; thus controlling the flexibility of cell-cell and free cell boundaries, respectively (Fig. 3).

The ability of a leader cell to pull a sprout depends on the interplay between the surface tension of the aggregate, β, and the propulsion strength P. For large enough β the increase in the perimeter of the area encompassed by the cell blocks the forward movement of the sprout tip. On the other hand, if the propulsion strength P is too large, the tip cell moves too fast for the passive cells to respond. Thus, for each set of CPM parameter values we determined the lowest propulsion strength P that still leads to a (slow) sprout expansion.

In simulations performed with minimal sprout expansion speeds the leader cell deforms the shape of the aggregate and pulls a few passive cells into the forming sprout. Then, the sprout length is increased at the expense of its width – reminiscent e.g., to the reported dynamics of tracheal tube formation in fruit flies [32]. However, after the sprout has sufficiently narrowed, cell-cell connections break: passive cells are pulled back to the initial aggregate leaving the leader cell, and possibly a few passive cells, in a separate cluster. As Fig. 3 demonstrates, the sprout at its maximal length contains 3-4 cells on average.

The maximum sprout length increases with β (the penalty associated with free cell surfaces) and slightly decreases for increasing α. The decrease in α allows for more interdigitated and hence stable cell-cell contacts. Increasing the surface tension of the cell clusters, β, yields more compact aggregates and thicker sprout bases. When $\beta < \alpha/2$, cells dissociate from the aggregate and diffuse freely on the substrate.

The inability of surface tension to maintain a sprout can be seen by simple geometrical arguments. Due to the similarity between cell-cell adhesion and surface tension [11] we only need to compare cell perimeter lengths and their associated CPM Hamiltonian (3.2) in a long sprout of width d and at a surface of an aggregate (Fig. 4). For simplicity we consider only rectangular cells at their target area A, but the argument can be easily extended to more complex shapes. A cell located at the surface of an aggregate contributes

$$H_{surface}(d) = \frac{A\alpha}{d} + (\alpha/2 + \beta)d \tag{5.1}$$

to the CPM Hamiltonian, as borders between cells are accounted for twice. Since a cell at the surface can adjust its width to minimize H, its contribution becomes

$$H_{surface} = \sqrt{2A\alpha(\alpha + 2\beta)}. \tag{5.2}$$

In contrast, the width of a cell in a sprout is set by the sprout thickness, and the corresponding contribution to (3.2) is

$$H_{sprout}(d) = \frac{2A\beta}{d} + \alpha d. \tag{5.3}$$

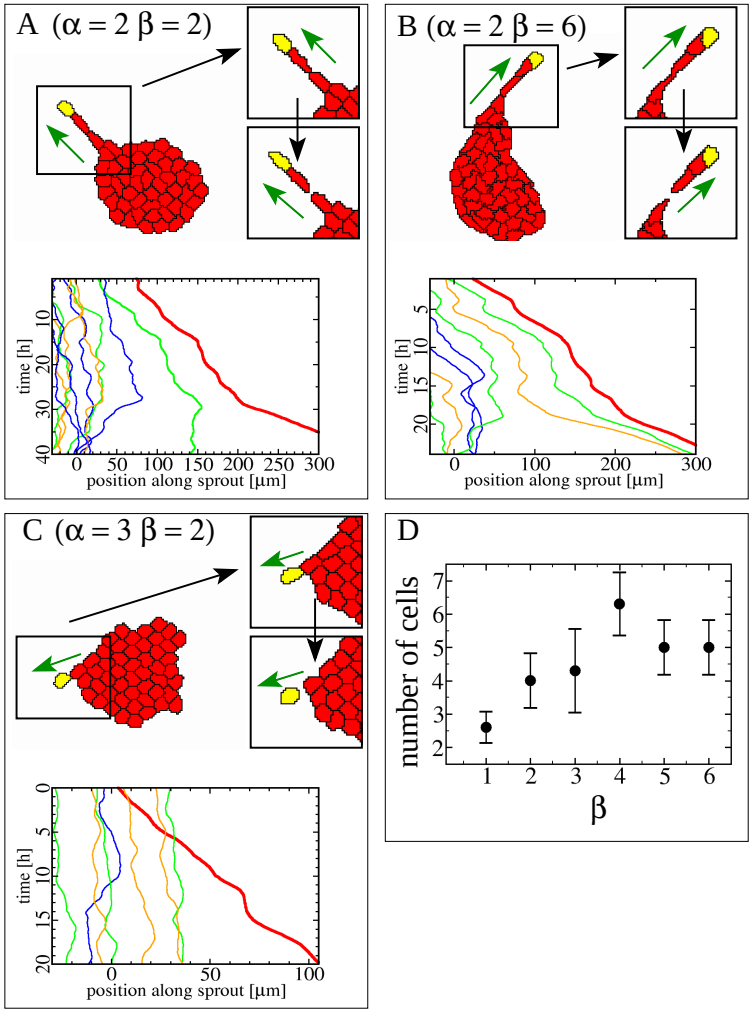

Figure 3: Leader cells are unable to sustain cell recruitment to the sprout from the initial aggregate by cell-cell adhesion alone. In the simulations tip cells eventually detach from the sprouts – as shown in the insets – irrespective of surface tension parameters. Green arrows mark the direction of sprout extension, black arrows indicate time-sequence. The self-propulsion parameter P was set to yield minimal sprout elongation speeds. Trajectory plots in each panel show cell movements along the sprout axis. A, B: low and high costs associated to free cell boundaries ($\alpha = 2, \beta = 2, P = 2$) and ($\alpha = 2$, $\beta = 6$, $P = 7$), respectively. Larger β values result in a thick initial bulge and longer sprout extension. Passive cells retract after the sprout breaks – a process driven by the elastic energy accumulated in the sprout. C: An increased cost associated to cell-cell boundaries (α) results in smoother and shorter contact areas ($\alpha = 3$, $\beta = 2$, $P = 1$). Due to the reduced contact surface cell-cell connections break more easily. D: The number of cells incorporated in the sprout at its maximal extent was determined for $\alpha = 1$ and various values of the parameter β. All data points are an average obtained from three independent runs, the errorbars represent standard deviations.

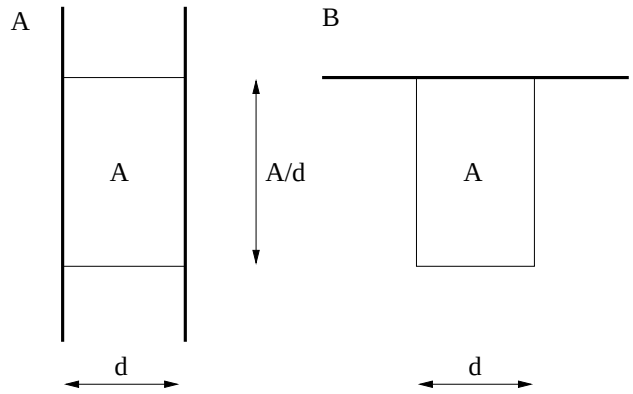

Figure 4: Comparison of cells in two configurations. A cell of width d within a linear sprout (A) and a similar cell at the surface of an aggregate (B). Thick and thin lines represent free and cell-cell boundaries, respectively.

If $\beta > \alpha/2$, it is easy to show that for arbitrary d:

$$H_{sprout}(d) \geq 2\sqrt{2A\alpha\beta} > H_{surface}. \tag{5.4}$$

Thus, a cell always prefers to be at the surface of an aggregate, rather than in a sprout – which blocks surface-tension driven cell recruitment at the sprout base.

5.2. Spontaneous sprout formation in a model with preferential attachment to elongated cells

We suggested previously that sprouts could be stabilized by preferential attraction to elongated cells [46] and a simpler CPM system ($w_1 \equiv 0$ and $w_2 \equiv 0$) was explored with simulations [45]. As $w_3 \neq 0$, the dynamics of the whole system is not a surface tension-driven relaxation process towards equilibrium. However, the motion of a single cell in a given environment is still governed by effective surface energies (see Eq. (9) in [45]). The lower effective surface energy (α) values associated with contacts on elongated sprout cells decreases expression (5.3). Preferential attraction to elongated cells, therefore, can offset the penalty for long free boundaries, and thus invalidate the instability condition (5.4).

In similar systems without leader cells but with $w_i \neq 0$ for $i = \{1, 2, 3\}$, random fluctuations in cellular motility can initiate spontaneous sprouts by displacing a cell from an aggregate (Fig. 5). Since the displaced cell continues to attach to the aggregate, it assumes an elongated shape which attracts additional cells into the sprout. This spontaneous sprouting process – i.e., without specialized leader cells – is heavily influenced by the strength of surface tension β. If the surface tension is low, free cell surfaces fluctuate more and it is easier for the cells to leave the aggregate. Thus, the unrealistic jagged appearance of cell surfaces is connected with the possibility that such sprouts can develop. Furthermore, irrespective of the strength of surface tension, long sprouts cannot be

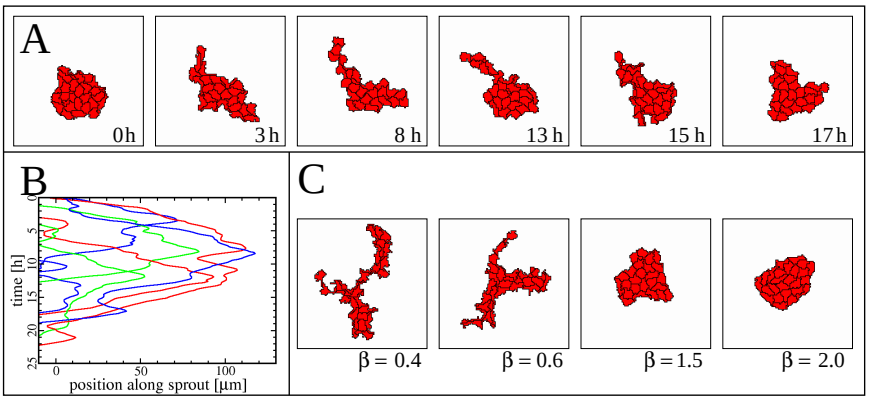

Figure 5: Spontaneous sprouting without leader cells. A: time-course of sprout growth. Several elongated cells form a several cell-diameter long, transient sprout ($\alpha = 2$, $\beta = 1$, $P = 4$, $\chi = 5$). The lifetime of the sprout is ≈15 hours. B: cell movements in the sprout shown in panel A are depicted as trajectories. C: the surface energy of free cell boundaries (β) is a key determinant of sprout shape. High values of β keep the cells together in the initial aggregate. Lowering β increases cell surface fluctuations and cells can break away from the aggregate more frequently ($\alpha = 2$, $P = 4$, $\chi = 5$).

maintained without the tip's attachment to another group of cells. The jagged sprout surfaces and their limited lifetime, however, does not match the experimentally observed structures and dynamics shown in Fig. 1.

5.3. Leader cells and preferential attraction

The unrealistic cell shape and sprout behavior that emerge from the simulations shown in Fig. 5 are partly consequences of ignoring some basic properties of cell motility, such as localized protrusion activity in the front of the cells or directional persistence of cell motility. Furthermore, the motile state of sprout cells is clearly different from those in the aggregate, thus it is reasonable to include leader and passive cells in the model.

Simulations of the full model, i.e., with leader cells ($P = 4$, $T = 500$MCS), preferential attraction to elongated cells ($\chi = 3$) and localization of membrane protrusions to the leading edge ($S = 2$, $\psi = 0.1$) yield sprouting dynamics comparable to that of experimental results (Fig. 6). Thus, leader cells are able to leave the initial aggregate, then form and maintain an expanding sprout by recruiting passive cells at the sprout base. The shape of the sprout as well as its expansion speed is determined by the persistence time of the leader cell. In particular, faster expansion increases cell elongation, which helps to recruit additional cells at the sprout base.

The effect of localizing the elementary steps to leading edges is demonstrated in Fig. 7. For $S > 0$, spin conversions at the leading edge are accepted more frequently. As a consequence, cells become elongated in the direction of their movement which helps recruit cells to the sprout.

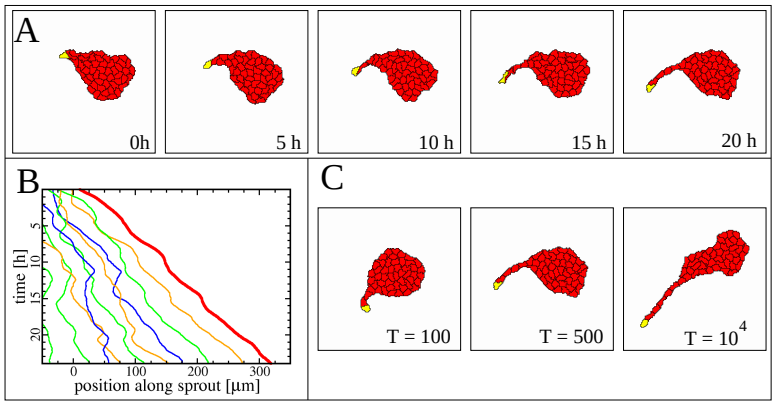

Figure 6: Leader-cell initiated sprouting behavior in a system with preferential attraction to elongated cells. A: typical time-course of sprout growth: the leader is slightly elongated, thus it pulls passive cells from the initial aggregate. The passive cells become elongated as well and attract further cells into the growing sprout. With sufficient supply of cells, the expansion can continue for an extended time period ($\alpha = 2$, $\beta = 2$, $P = 4$, $T = 500$MCS, $\chi = 3$, $S = 2$, $\psi = 0.1$). B: cell trajectories along the sprout direction reveal cells entering the sprout as well as changes in cell order due to differential motion in the sprout. C: persistence time of polarity defines sprout shape and length, through the polarity persistence parameter T. When the leader cell is more persistent, longer and straighter sprouts form.

6. Discussion

Sprouting is a collective cellular phenomenon exhibited by several types of tissue cells: avian vasculogenesis [39] and *Drosophila* trachea formation [32] represent two well-studied examples during embryonic development. Collective chain migration is also ubiquitous during tumor invasion [14], as well as in cell cultures (both 3D [15] and 2D [45]). Cell-cell contacts also seem to play a role in neural crest cell migration [47]. Thus, empirical evidence suggest that multicellular sprout formation is a general ability of a wide variety of tissue cells.

In this paper we argued that sprout elongation is likely to involve active cellular motility, guided by cell-cell contacts. Furthermore, cell surfaces in the sprout must be more attractive than surfaces of well-spread cells in the aggregate bulk. A plausible mechanism resulting in this behavior could involve the detection of micromechanical properties characteristic for elongated sprout cells[26]. Mechano-sensing of extracellular matrix stiffness has been demonstrated in several cell types [28, 20, 25]. An analogous mechano-sensing of cell surfaces is also feasible. For example, VE-cadherin, a major cell-cell adhesion receptor of vascular endothelial cells, was recently shown to be incorporated in cell surface mechano-sensing complexes [48]. The altered composition of cell surface-attached ECM could provide an alternative mechanism to distinguish sprout cell surfaces [15].

Here we also proposed that leader and passive cells differ in their persistence of cell polarity. Similar results are obtained when the the self-propulsion coefficient P differs between leader and

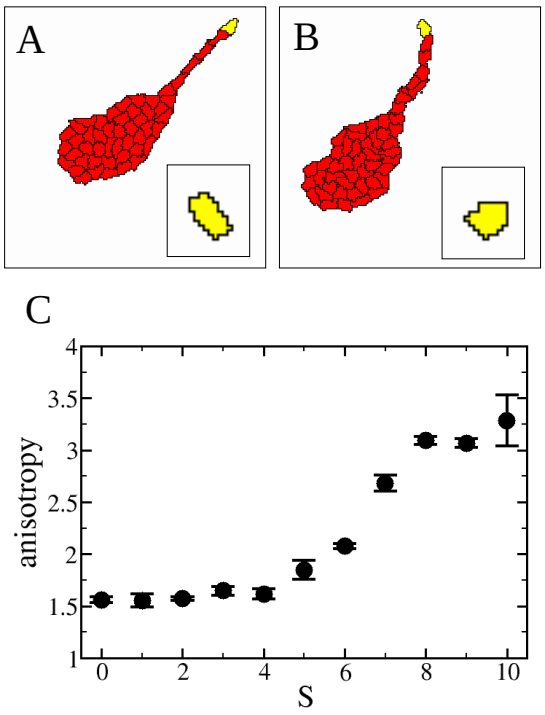

Figure 7: The effect of restricting elementary steps (membrane fluctuations) to the leading edge. A: for $S = 4$, $\psi = 0.1$, $P = 4$, motile cells are elongated (inset) which contributes to the sprouting process ($\alpha = 2$, $\beta = 2$). B: as a comparison, for $S = 0$ and $P = 4$ the disk-shaped cells recruit cells less efficiently resulting in slower elongation of the sprout ($\alpha = 2$, $\beta = 2$). C: the shape change of non-interacting leader-type cells is characterized by their anisotropy θ.

passive cells (data not shown). Currently there is no empirical data available on the motility difference between these cell phenotypes at the level of an *isolated* cell. It is also unknown if and how long leader cells maintain their behavior when isolated from the rest of the system, or whether cell behaviors can alternate between passive and leader states, and – if so – what affects this transition.

The model investigated here results in sprouts that are (i) able to recruit cells from the base, and (ii) are linear structures (iii) with a steady expansion speed. Furthermore, (iv) cells in the sprout can mix and change their order. To achieve this behavior we needed both persistently moving tip cells as well as preferential adhesion to elongated cells. The duration of cell polarity in leader cells, $T \approx 6h$ is long, however individual endothelial cells can exhibit a persistence time of several hours in low cell density culture [43].

Another, widely considered sprout-guidance mechanisms involve chemotaxis [16, 42, 30, 2, 31, 3] or mechanotaxis probing the ECM environment. The latter assumes that cells exert mechanical stress on the underlying substrate, and the resulting strain guides cellular motility [34, 33, 29, 40]. Lateral migration of cells can also be limited by ECM fragments [15], ECM-bound guidance cues such as VEGF isoforms or semaphorins [22]. Cadherin-independent cell-cell adhesions, such as

tight junctions are also expected to behave differently from the liquid droplet models, in which the relative movement between adjacent cell bodies is irrelevant as long as the size of their contact surface is preserved. The integration of these cellular mechanisms into a mechanistic model of sprout elongation remains an exciting goal.

Acknowledgements

We are grateful to Roeland H Merks for generously sharing his simulation code with us at `http://sourceforge.net/projects/tst`. This work was supported by the NIH (R01 HL87136), the American Heart Association (SDG 0535245N) and the Hungarian Science Fund (OTKA K72664).

References

[1] M. Alber, N. Chen, T. Glimm, P. M. Lushnikov. *Multiscale dynamics of biological cells with chemotactic interactions: from a discrete stochastic model to a continuous description*. Phys. Rev. E Stat. Nonlin. Soft Matter Phys., 73 (2006), No. 5/1, 051901.

[2] A. L. Bauer, T. L. Jackson, Y. Jiang. *A cell-based model exhibiting branching and anastomosis during tumor-induced angiogenesis*. Biophys. J., 92 (2007), No. 9, 3105–3121.

[3] A. L. Bauer, T. L. Jackson, Y. Jiang. *Topography of extracellular matrix mediates vascular morphogenesis and migration speeds in angiogenesis*. PLOS Comp. Biol., (in press), 2009.

[4] J. M. Belmonte, G. L. Thomas, L. G. Brunnet, R. M. C. de Almeida, H. Chaté. *Self-propelled particle model for cell-sorting phenomena*. Phys. Rev. Lett., 100 (2008), No. 24, 248702.

[5] D. A. Beysens, G. Forgacs, J. A. Glazier. *Cell sorting is analogous to phase ordering in fluids*. PNAS, 97 (2000), 9467–71.

[6] A. Czirók, E. A. Zamir, A. Szabó, C. D. Little. *Multicellular sprouting during vasculogenesis*. Curr. Top. Dev. Biol., 81 (2008), 269–289.

[7] A. T. Dawes, L. Edelstein-Keshet. *Phosphoinositides and rho proteins spatially regulate actin polymerization to initiate and maintain directed movement in a one-dimensional model of a motile cell*. Biophys. J., 92 (2007), No. 3, 744–768.

[8] P. G. de Gennes, F. Brochard-Wyart, D. Quere. *Capillarity and wetting phenomena*. Springer, New York, 2003.

[9] A. Dipasquale. *Locomotion of epithelial cells. Factors involved in extension of the leading edge*. Exp. Cell Res., 95 (1975), No. 2, 425–439.

[10] O. du Roure, A. Saez, A. Buguin, R. H. Austin, P. Chavrier, P. Silberzan, B. Ladoux. *Force mapping in epithelial cell migration*. Proc. Natl. Acad. Sci. U S A, 102 (2005), No. 7, 2390–2395.

[11] G. Forgacs, R. A. Foty, Y. Shafrir, M. S. Steinberg. *Viscoelastic properties of living embryonic tissues: a quantitative study*. Biophys. J., 74 (1998), No. 5, 2227–2234.

[12] R. A. Foty, C. M. Pfleger, G. Forgacs, M. S. Steinberg. *Surface tensions of embryonic tissues predict their mutual envelopment behavior*. Development, 122 (1996), No. 5, 1611–1620.

[13] R. A. Foty, M. S. Steinberg. *The differential adhesion hypothesis: a direct evaluation*. Dev. Biol., 278 (2005), No. 1, 255–263.

[14] P. Friedl. *Dynamic imaging of cellular interactions with extracellular matrix*. Histochem. Cell Biol., 122 (2004), 183–90.

[15] P. Friedl, K. Wolf. *Tube travel: the role of proteases in individual and collective cancer cell invasion*. Cancer Res., 68 (2008), No. 18, 7247–7249.

[16] A. Gamba, D. Ambrosi, A. Coniglio, A. de Candia, S. Di Talia, E. Giraudo, G. Serini, L. Preziosi, F. Bussolino. *Percolation, morphogenesis, and burgers dynamics in blood vessels formation*. Phys. Rev. Lett., 90 (2003), No. 11, 118101.

[17] H. Gerhardt, M. Golding, M. Fruttiger, C. Ruhrberg, A. Lundkvist, A. Abramsson, M. Jeltsch, C. Mitchell, K. Alitalo, D. Shima, C. Betsholtz. *Vegf guides angiogenic sprouting utilizing endothelial tip cell filopodia*. J. Cell Biol., 161 (2003), No. 6, 1163–1177.

[18] J. A. Glazier, F. Graner. *Simulation of the differential adhesion driven rearrangement of biological cells*. Phys. Rev. E Stat. Phys. Plasmas Fluids Relat. Interdiscip. Topics, 47 (1993), No. 3, 2128–2154.

[19] F. Graner, J. A. Glazier. *Simulation of biological cell sorting using a two-dimensional extended potts model*. Phys. Rev. Lett., 69 (1992), No. 13, 2013–2016.

[20] D. S. Gray, J. Tien, C. S. Chen. *Repositioning of cells by mechanotaxis on surfaces with micropatterned young's modulus*. J. Biomed. Mater. Res. A., 66 (2003), 605–14.

[21] B. Hegedüs, F. Marga, K. Jakab, K. L. Sharpe-Timms, G. Forgacs. *The interplay of cell-cell and cell-matrix interactions in the invasive properties of brain tumors*. Biophysical J., 91 (2006), No. 7, 2708–16.

[22] K. A. Hogan, V. L. Bautch. *Blood vessel patterning at the embryonic midline*. Curr. Top. Dev. Biol., 62 (2004), 55–85.

[23] M. S. Hutson, G. W. Brodland, J. Yang, D. Viens. *Cell sorting in three dimensions: topology, fluctuations, and fluidlike instabilities*. Phys. Rev. Lett., 101(2008), No. 14, 148105.

[24] J. A. Izaguirre, R. Chaturvedi, C. Huang, T. Cickovski, J. Coffland, G. Thomas, G. Forgacs, M. Alber, G. Hentschel, S. A. Newman, J. A. Glazier. *Compucell, a multi-model framework for simulation of morphogenesis*. Bioinformatics, 20(2004), No. 7, 1129–1137.

[25] G. Jiang, A. H. Huang, Y. Cai, M. Tanase, M. P. Sheetz. *Rigidity sensing at the leading edge through alphavbeta3 integrins and rptpalpha*. Biophys J., 90 (2006), 1804–9.

[26] S. Kidoaki, T. Matsuda. *Shape-engineered fibroblasts: cell elasticity and actin cytoskeletal features characterized by fluorescence and atomic force microscopy*. J. Biomed. Mater. Res. A., 81 (2007), No. 4, 803–810.

[27] T. Libotte, H. W. Kaiser, W. Alt, T. Bretschneider. *Polarity, protrusion-retraction dynamics and their interplay during keratinocyte cell migration*. Exp. Cell Res., 270 (2001), No 2, 129–137.

[28] C. M. Lo, H. B. Wang, M. Dembo, Y. L. Wang. *Cell movement is guided by the rigidity of the substrate*. Biophys J., 79 (2000), No. 1, 144–152.

[29] D. Manoussaki, S. R. Lubkin, R. B. Vernon, J. D. Murray. *A mechanical model for the formation of vascular networks in vitro*. Acta Biotheor, 44 (1996), No. 3-4, 271–282.

[30] R. M. Merks, S. V. Brodsky, M. S. Goligorksy, S. A. Newman, J. A. Glazier. *Cell elongation is key to in silico replication of in vitro vasculogenesis and subsequent remodeling*. Dev. Biol., 289 (2006), 44–54.

[31] R. M. H. Merks, E. D. Perryn, A. Shirinifard, J. A. Glazier. *Contact-inhibited chemotaxis in de novo and sprouting blood-vessel growth*. PLoS Comput. Biol., 4 (2008), No. 9, e1000163.

[32] D. J. Montell. *Morphogenetic cell movements: diversity from modular mechanical properties*. Science, 322 (2008), No. 5907, 1502–1505.

[33] J. D. Murray. Mathematical Biology. Springer Verlag, Berlin, 2nd edition, 2003.

[34] J. D. Murray, D. Manoussaki, S. R. Lubkin, R. Vernon. *A mechanical theory of in vitro vascular network formation*. In C. D. Little, V Mironov, and E. H. Sage, editors, Vascular morphogenesis: In vivo, in vitro, in mente., pages 223–239. Birkhauser, Boston, 1998.

[35] T. J. Newman. *Modeling multicellular systems using subcellular elements*. Math. Biosci. Eng., 2 (2005), 611–622.

[36] E. D. Perryn, A. Czirók, C. D. Little. *Vascular sprout formation entails tissue deformations and ve-cadherin-dependent cell-autonomous motility*. Dev. Biol., 313 (2008), 545–55.

[37] A. J. Ridley, M. A. Schwartz, K. Burridge, R. A. Firtel, M. H. Ginsberg, G. Borisy, J. T. Parsons, A. R. Horwitz. *Cell migration: integrating signals from front to back*. Science, 302 (2003), No. 5651, 1704–1709.

[38] J. P. Rieu, A. Upadhyaya, J. A. Glazier, N. B. Ouchi, Y. Sawada. *Diffusion and deformations of single hydra cells in cellular aggregates*. Biophys J., 79 (2000), 1903–14.

[39] P. A. Rupp, A. Czirók, C. D. Little. *alphavbeta3 integrin-dependent endothelial cell dynamics in vivo*. Development, 131 (2004), No. 12, 2887–97.

[40] R. K. Sawhney, J. Howard. *Slow local movements of collagen fibers by fibroblasts drive the rapid global self-organization of collagen gels*. J. Cell Biol., 157 (2002), No. 6, 1083–1091.

[41] D. Selmeczi, S. Mosler, P. H. Hagedorn, N. B. Larsen, H. Flyvbjerg. *Cell motility as persistent random motion: theories from experiments*. Biophys J., 89 (2005), 912–31.

[42] G. Serini, D. Ambrosi, E. Giraudo, A. Gamba, L. Preziosi, F. Bussolino. *Modeling the early stages of vascular network assembly*. EMBO J., 22 (2003), 1771–9.

[43] C. L. Stokes, D. A. Lauffenburger, S. K. Williams. *Migration of individual microvessel endothelial cells: stochastic model and parameter measurement*. J. Cell Sci., 99 (1991), 419–30.

[44] A. Szabó, R. Ünnep, E. Méhes, W. Twal, S. Argraves, Y. Cho, A. Czirók. *Collective cell motion in endothelial monolayers*. (preprint)

[45] A. Szabó, E. Méhes, E. Kósa, A. Czirók. *Multicellular sprouting in vitro*. Biophys J., 95 (2008), No. 6, 2702–2710.

[46] A. Szabó, E. D. Perryn, A. Czirók. *Network formation of tissue cells via preferential attraction to elongated structures*. Phys. Rev. Lett., 98 (2007), No. 3, 038102.

[47] J. M. Teddy, P. M. Kulesa. *In vivo evidence for short- and long-range cell communication in cranial neural crest cells*. Development, 131 (2004), No. 24, 6141–6151.

[48] E. Tzima, M. Irani-Tehrani, W. B. Kiosses, E. Dejana, D. A. Schultz, B. Engelhardt, G. Cao, H. DeLisser, M. A. Schwartz. *A mechanosensory complex that mediates the endothelial cell response to fluid shear stress*. Nature, 437 (2005), No. 7057, 426–431.

[49] A. Upadhyaya, J.-P. Rieu, J. A. Glazier, Y. Sawada. *Anomalous diffusion and non-gaussian velocity distribution of hydra cells in cellular aggregates*. Physica A, 293 (2001), 549–558.

[50] A. B. Verkhovsky, T. M. Svitkina, G. G. Borisy. *Self-polarization and directional motility of cytoplasm*. Curr. Biol., 9 (1999), No. 1, 11–20.